SSC20-VII-06

Optical Modeling, Alignment, and Testing for the Deformable Mirror Demonstration Mission (DeMi) CubeSat Payload

Rachel Morgan
Massachusetts Institute of Technology
77 Massachusetts Ave, Cambridge MA 02139; +1 617-253-7805
remorgan@mit.edu

Faculty Advisor: Professor Kerri Cahoy

ABSTRACT

Microelectromechanical Systems (MEMS) Deformable Mirrors (DMs) are a promising technology to enable the wavefront control required for high contrast imaging and characterization of exoplanets with coronagraph instruments. MEMS DMs are a key technology option for future exoplanet imaging space telescopes because they can provide precise wavefront control with low size, weight, and power required. The Deformable Mirror Demonstration Mission (DeMi) is flying a MEMS DM-based adaptive optics instrument on a CubeSat in order to demonstrate this technology in the space environment for the first time. The DeMi payload will characterize the on-orbit performance of a 140 actuator MEMS DM with 5.5 μm maximum stroke, with a goal of measuring individual actuator wavefront displacement contributions to a precision of 12 nm. The payload will be able to measure low order aberrations to $\lambda/10$ accuracy and $\lambda/50$ precision, and will correct static and dynamic wavefront phase errors to less than 100 nm RMS. The DeMi payload contains both a Shack Hartmann wavefront sensor and an image plane wavefront sensor to monitor the DM behavior on orbit. This paper describes an optical diffraction model of the payload and the flight payload alignment and integration process. The optical model is validated with relevant data from the flight payload. The DeMi satellite was launched successfully to the International Space Station on February 15, 2020 and deployment is expected in early Summer 2020.

Introduction

The Deformable Mirror Demonstration Mission (DeMi) CubeSat payload was built at MIT in order to demonstrate a Microelectromechanical Systems (MEMS) Deformable Mirror (DM) in space for the first time and provide on-orbit operations data for future space telescope missions planning to use DMs for high-contrast imaging of exoplanets.

High-Contrast Imaging of Exoplanets

High-contrast imaging can enable detailed characterization of exoplanets[1] by providing precise astrometric data[2] and spectroscopic measurements for atmospheric characterization.[3] This data can be used to constrain the orbits of exoplanets[4] and detect biosignatures in the atmosphere in order to assess potential habitability.[5] High contrast imaging instruments can also be used to detect and characterize circumstellar debris disk structure, which is useful to understand solar system formation and evolution.[6]

Small, rocky, Earth-like planets are around a billion times dimmer than the stars they orbit, and tend to orbit at close angular separations to the star. This makes imaging and characterizing Earth-like planets an immense technical challenge. In order to resolve an Earth-like planet orbiting a Sun like star, a telescope instrument must be able to image the planet at extremely high contrasts of $\sim 10^{-10}$.[7] Achieving this contrast level with a coronagraph instrument, which blocks out the light of the target star so the dim companion planet is visible, requires an adaptive optics system capable of picometer-level wavefront control.[8] Deformable mirrors can be used to achieve this extreme wavefront control in coronagraph systems in order to prevent speckles and stray light from degrading the contrast.[8,9,10]

An adaptive optics system corrects wavefront errors in a telescope in order to improve image quality and contrast. It was first proposed in 1953 to correct for errors due to atmospheric turbulence for ground-based observatories.[11] For space telescopes, adaptive optics is proposed to correct wavefront errors due to thermal and mechanical effects in space. In an adaptive optics system, a wavefront sensor is

used to detect wavefront errors, which are corrected by controlling an adaptive or deformable mirror to counteract them. A deformable mirror can also be used to inject known perturbations into the system in order to probe the wavefront for common-path wavefront sensing.[12]

Microelectromechanical Systems (MEMS) DMs offer high-actuator density, large stroke, and precise control in a small, low-power form factor, which makes them suitable for space-based wavefront control applications. MEMS DMs are a promising technology option to enable the precise wavefront control required for exoplanet direct imaging with space telescope coronagraph instruments.[13,14] Other types of DM technology have been investigated for space applications, such lead magnesium niobate (PMN) piezolectric ceramics or voice-coil actuators. Other applications of MEMS DMs include biological imaging, free-space laser communications, or Earth observation.[15]

DeMi CubeSat Payload

The Deformable Mirror Demonstration Mission (DeMi) CubeSat payload will demonstrate the on-orbit performance of a 140-actuator BMC MEMS DM on a 6U (10 cm × 20 cm × 30 cm) CubeSat.[16,17,18,19,20] The goal of this mission is to raise the Technology Readiness Level (TRL) of MEMS DM technology from a TRL of 5 to at least a TRL of 7 for future space telescope applications.[21] The key DeMi mission requirements are to measure individual DM actuator wavefront displacement contributions to a precision of 12 nm, measure low order optical aberrations to $\lambda/10$ accuracy and $\lambda/50$ precision, and correct static and dynamic wavefront errors to less than 100 nm RMS error.

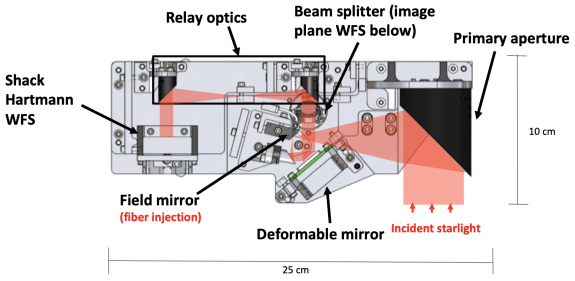

Figure 1: Diagram of the optical components for the Deformable Mirror Demonstration Mission (DeMi) CubeSat payload with ray path overlaid.

The DeMi optical design contains an off axis parabola-based telescope with a 50 mm primary mirror, a 140-actuator BMC Multi DM, and both an Image Plane wavefront sensor (WFS) and a Shack Hartmann WFS.[22] The Image Plane WFS captures pictures of the system Point-Spread Function (PSF) and serves as a truth sensor for wavefront correction. The Image Plane WFS is also used to detect tip-tilt errors. The Shack Hartmann WFS uses a lenslet array to split the light into sections and focus it into a grid of spots on the detector. The displacement of each spot corresponds to the wavefront slope incident on the corresponding lenslet. This sensor is used to measure wavefront aberrations and monitor the DM health on-orbit. A diagram of the DeMi optical payload is shown in Figure 1.

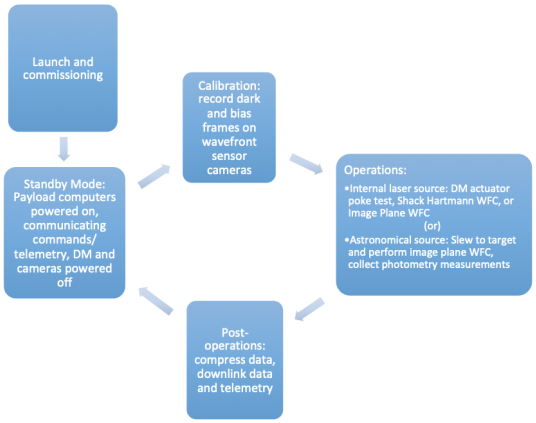

Figure 2: Summary of concept of operations for the Deformable Mirror Demonstration Mission. A DM actuator poke test refers to actuating each actuator of the deformable mirror in a sequence and measuring the deflection with the Shack Hartmann wavefront sensor in order to measure the behavior of the mirror over time. WFC stands for wavefront control using either the Shack Hartmann wavefront sensor or the image plane wavefront sensor.

A summary of the DeMi concept of operations is shown in Figure 2. The DeMi payload has both external and internal operational modes. It can observe stellar targets and collect photometric measurements through the primary aperture, or it can use the internal laser fiber source for calibration measurements. For external observations of stellar targets, the Image Plane WFS will be used for closed-loop control of the DM, and performance will be measured with the Shack Hartmann WFS. For internal calibration, the internal laser source will be turned on and either the Image Plane WFS or the

Shack Hartmann WFS will be used for closed-loop control of the DM, with the other sensor measuring performance. The internal laser source will also be used for actuator tests of the DM where each actuator will be poked and the resultant wavefront will be measured on both the Image Plane WFS and the Shack Hartmann WFS. This data will be used to assess the on-orbit performance of the MEMS DM over a year of operation.

This paper describes the development of an optical model of the DeMi payload. The alignment and integration of the flight payload are described, and measurements from the flight payload are compared to predictions from the optical model. The DeMi CubeSat was launched successfully to the International Space Station onboard the Northrop Grumman 13 mission in February 2020. Deployment from the Space Station and on-orbit operations are expected to begin in early Summer 2020.

Optical Diffraction Model

An optical diffraction model has been developed for the DeMi payload in order to predict measurements on both the image plane wavefront sensor and the Shack Hartmann wavefront sensor in response to actuator commands applied to the DM. This gives the DeMi team a baseline to compare with the payload data from ground testing and in-flight operations. The optical diffraction model is also useful to simulate the effect of the DM being inclined 45° relative to the incident beam in the payload on the wavefront sensor measurements for DM shapes. The DeMi design has the DM at a 45° inclination in order to save space in the optical bench to fit within the CubeSat form factor. The optical diffraction model was developed using the open-source Physical Optics Propagation in PYthon (POPPY) software package.[23]

The DeMi POPPY model is based on Fraunhofer diffraction integrals. This approach assumes that all diffraction effects in the payload are either in the "far-field" or are placed at principal planes (focal planes or pupil planes).[24] In the DeMi optical design this assumption is justified because all optical components are at principal planes. These assumptions greatly reduce the complexity of the diffraction integrals, making the optical model less computationally expensive. Fraunhofer diffraction is modeled by computing the two-dimensional Fourier transforms between image planes and pupil planes.[24]

POPPY models an optical wavefront as a python object with phase and amplitude stored in arrays. The optical system is modeled as a series of optical elements at principal planes, which are python objects defined by their transmittance and optical path difference (OPD) across the optical element, each also stored as arrays. POPPY propagates the optical wavefront between principal planes through a Matrix Fourier Transform to convert between spatial units in pupil planes and angular frequency units in image planes. At each optical element, the wavefront object phase and amplitude arrays are multiplied by the OPD and transmittance arrays of the optical element object. At the image plane detector, the wavefront is propagated to the detector plane and the intensity is computed then sampled to match the specified detector size and pixel pitch. At the Shack Hartmann wavefront sensor, the wavefront is subsampled to simulate the effect of the lenslet array. Then, each subsampled wavefront array is propagated to the detector plane separately then tiled back together to form simulated images of the detector spots. The Shack Hartmann wavefront sensor simulation used the sub-sampled optics object in POPPY, which was originally written by Ewan Douglas and was developed and validated through this work. The code used in work will be pushed to the official POPPY source code[1] in the future.

Table 1: DeMi optical design parameters relevant to the POPPY optical diffraction model.

Parameter	Value	Unit
Primary aperture Diameter	30	mm
Deformable mirror (DM) actuator pitch	450	μm
DM actuators per side	12	
Internal calibration laser wavelength	635	nm
Camera pixel pitch	2.2	μm
Image plane detector field of view (full angle)	1.9	deg
Image plane detector plate scale	2.7	arcsec/pixel
Shack Hartmann number of lenslets across DM	36	
Shack Hartmann detector lenslet pitch	150	μm
Shack Hartmann detector lenslet focal length	3.7	mm

The DeMi optical payload design is shown in Figure 1. Following the ray trace in this figure, the design can be represented by a series of optics at principal planes. The primary aperture (OAP1) is at a pupil plane, the field mirror is at an image

[1] https://github.com/spacetelescope/poppy

plane, OAP2 is a at a pupil plane, the DM is at a pupil plane, and the image plane focusing lens is at a pupil plane which focuses the light onto the detector in an image plane. Continuing onto the relay optics, OAP3 is at a pupil plane, there is an image plane between OAP3 and OAP4, OAP4 is at a pupil plane, and the Shack Hartmann lenslet array is at a pupil plane. Each lenslet in this array focuses the subsampled wavefront onto the detector in the image plane. The POPPY model uses flight-like parameters to define the optical system, summarized in Table 1.

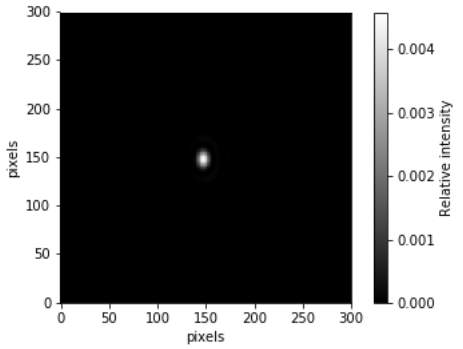

Image plane PSF simulation

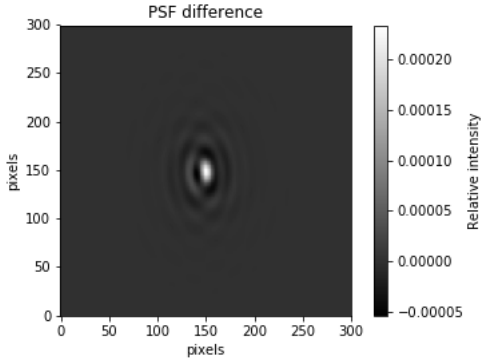

Poked DM output subtracted from flat DM output

Figure 3: Image plane wavefront sensor POPPY model with [3,5] actuator poked to 0.27 μm. (Top) POPPY output image zoomed in to see the PSF. (Bottom) Difference between POPPY output with flat DM and with poked actuator.

The POPPY model was used to simulate the Point Spread Function (PSF) on the image plane wavefront sensor by propagating the input wavefront up to the beam splitter and then reflecting and focusing the wavefront onto the image plane detector. To determine the size of the nominal PSF, a Gaussian function was fit to the model output. The measured size of the PSF Gaussian fit was 3.7 pixels in x and 5.3 pixels in y. The elliptical shape of the PSF is due to the inclination of the DM in the optical path. A sample result from the POPPY model for a single actuator poke applied to the DM is included in Figures 3. This image plane wavefront sensor simulation is very quick to run, typically taking 6-7 seconds on a 2017 MacBook Pro as measured by Python's timeit() function.

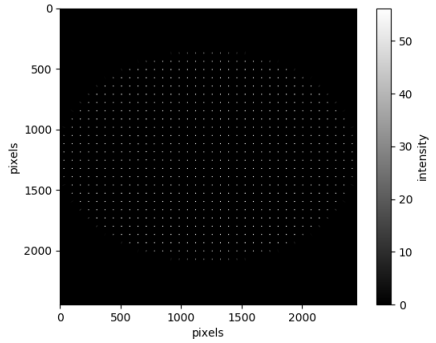

SHWFS simulation result

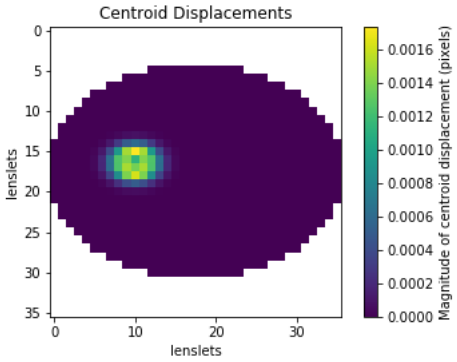

Centroid displacements

Figure 4: Example output of the Shack Hartmann POPPY model for a DM with the [3,5] actuator poked to 0.27 μm (top). The effects of these pokes is not visible to the eye, but can be seen in the centroid displacements shown on the bottom. The centroid displacement plot shows the magnitude of the displacement of each lenslet from its nominal position with a flat DM.

The POPPY model was also used to simulate the spots on the Shack Hartmann wavefront sensor. The POPPY model simulates this by propagating the light through the DeMi optical system (transmitting through the beam splitter to reach the Shack Hartmann optics) and then subsampling the wavefront so the light incident upon each lenslet in the

lenslet array optic is focused onto the detector individually. Each spot PSF is calculated individually and then tiled together to form the spot field. The large number of lenslets in the DeMi system caused the wavefront object to have very large arrays to keep track of the phase and amplitude along the optical path, which makes the Shack Hartmann simulation computationally intensive. The DeMi POPPY model was run on the MIT Engaging cluster at the MGHPCC facility (www.mghpcc.org) and the Shack Hartmann calculations typically took 5 minutes to run.

The DeMi POPPY model was used to simulate the spot field on the Shack Hartmann wavefront sensor. The size of each lenslet spot was determined by fitting a Gaussian function to a single focused lenslet spot, and the measured spot size was 2.9 pixels in diameter. The POPPY model was used to simulate Shack Hartmann wavefront sensor measurements for single actuator pokes. Figure 4 shows example output for the [3,5] actuator poked to 0.27 μm.

The Shack Hartmann spot fields were then processed to reconstruct the wavefront. First, the centroids of each spot in the spot field were calculated. Then, centroids from a simulation with a flat DM were subtracted from the centroids with a perturbed DM to find the difference due to the DM shape. The Moore-Penrose pseudoinverse approach is used for zonal reconstruction of the wavefront according to the Southwell geometry implementation[25] described in Dai 2008.[26] The gaussfitter python package was used to fit a gaussian to the poke measurement.[2] The height of the gaussian fit was used as the actuator deflection height to compare to physical data. Reconstructed wavefronts for the spot field shown in Figure 4 are shown in Figure 5. For the 270 nm actuator poke simulation, the actuator deflection measured was 240.7 nm, which is 90% of the input actuator displacement, and the residual had a median of 1.2e-4 um and a standard deviation of 2.6e-3 um. The small residual level shows that the Gaussian fits are a good way to retrieve the actuator deflection measurement from the data. The wavefronts and gaussian fits in Figure 5 are reported in units of wavefront error, which are divided by two to convert to physical units to calculate the actuator deflection.

Flight Payload Alignment

The DeMi CubeSat optical payload was assembled and aligned using a Zygo interferometer. The DeMi payload was aligned to a requirement of 0.25 waves RMS wavefront error. The preliminary alignment procedures for the engineering model are described in detail in Gubner 2018[27] and the final flight alignment is summarized here. Jennifer Gubner, Ewan Douglas, Yinzi Xin, and Gabor Furesz contributed significantly to the alignment procedures used for DeMi.

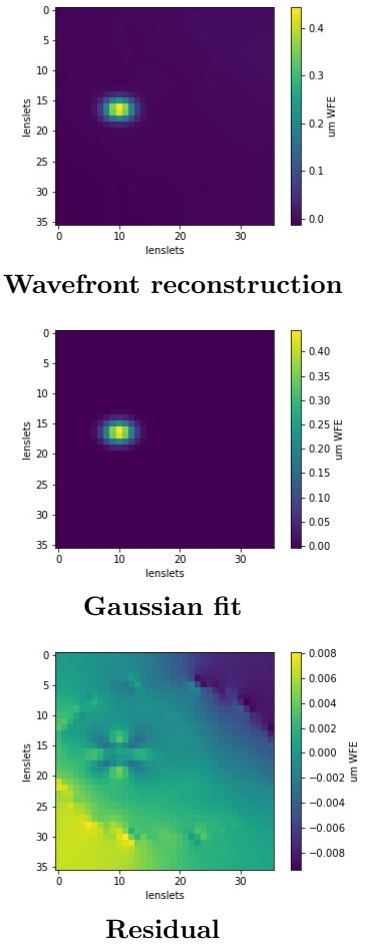

Figure 5: Data analysis for POPPY simulation shown in Figure 4 for the [3,5] actuator poked to 0.268 um. The reconstructed wavefront is shown on the top, the Gaussian fit to the reconstruction is in the center, and the residual between the data and the measurement (reconstruction subtracted from Gaussian fit in this case) is shown on the bottom. The height of the Gaussian fit is used as the measured actuator deflection to compare to the input setting.

The DeMi payload alignment split the payload into sections of one or more optical elements that

[2] https://github.com/keflavich/gaussfitter

were aligned as a section, then aligned within the full optical system. The sections were (using the labeling convention from Figure 1): OAP1 (the primary mirror), field mirror bench (consisting of the field mirror and OAP2), DM (the deformable mirror and its mount), the beam splitter (the beam splitter mount which the image plane lens and camera mount attaches to), the relay bench (consisting of OAP3 and OAP4), and the Shack Hartmann wavefront sensor (consisting of the lenslet array mount and the Shack Hartmann camera).

First, all of the optics were mounted or bonded into place and assembled onto their benches. The OAP optics and DMs were mounted to their mounts with screws. A setup DM was used in place of the flight DM during initial alignment to protect the flight DM from damage. The beamsplitter, image plane lens, and Shack Hartmann lenslet array optics were bonded to their mounts with RTV566. The optical fiber for the calibration laser was cleaved and installed into the groove within the field mirror and staked into place using 3M Epoxy Adhesive EC2216. The optical fiber was threaded through a teflon tube which was staked to the fiber output hole in the field mirror mount to protect the fiber during alignment and integration. This optical fiber had an FC/PC connector at the end which allowed us to plug it into a laser to test the optical path of the internal laser source throughout alignment. After alignment, the FC/PC connector end was removed and the flight laser was spliced into place.

Then, the relay bench was aligned by removing OAP4 and installing the relay bench on a tip-tilt and rotation stage in front of the Zygo. OAP3 was aligned to the Zygo using a spherical retroreflector on a translation stage and adjusting tip/tilt/rotation of the relay bench to reduce the RMS wavefront error to less than 0.25 waves. Then, OAP4 was reinstalled and a retroreflector was used to measure the total wavefront error of the full relay. The bushings on the OAP4 mount were adjusted to remove the error caused by misalignment between OAP3 and OAP4 so that the total RMS wavefront error was less than 0.25 waves.

Next, the field mirror assembly was aligned by attaching the optical fiber that was installed into the slot in the field mirror to a laser and using a shear plate interferometer to test the collimation after the light reflected off of OAP2. The bushings between the field mirror and the field mirror mount were adjusted until the shear plate interferometer measurement indicated that the light reflected off of OAP2 was well collimated. A picture of the aligned field mirror assembly with the optical fiber installed is shown in Figure 6.

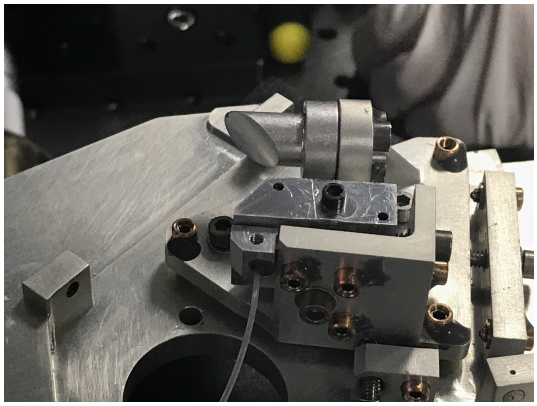

Figure 6: Aligned field mirror/OAP 2 assembly with optical fiber installed and epoxied into place.

At this point, OAP1 was installed into the flight deck and mounted on tip/tilt stages in front of the Zygo interferometer. The OAP was aligned to the interferometer by using a spherical retroreflector to reflect the focused beam off of OAP1 back into the interferometer and adjusting the tip/tilt stage until the errors from misalignment between the OAP1 and interferometer were minimized. The spherical retroreflector was mounted on a linear translation stage along the output optical axis of the OAP to aid in alignment of the spherical retro in the system.

Once OAP1 was aligned to the interferometer, the field mirror assembly was installed. A corner-cube retroreflector was used to reflect the light back into the interferometer, and the bushings controlling the tip, tilt, and rotation of the field mirror assembly were adjusted to minimize the errors caused by misalignment between OAP1 and the field mirror assembly.

Then, a setup-grade DM was installed into the DM mount and installed into the payload to check the spot location on the mirror. The setup-grade DM is a non-operational Multi DM from BMC with the same form factor as the flight-grade and engineering-grade DMs. For DeMi, the goal was to have the laser spot as centered on the DM as possible. The DM mount had a tendency to cant forward when the screws were torqued, so washers were used as shims to support the DM mount and prevent this behavior. Once the DM mount was installed into a good location, the setup-grade DM was swapped for the actual flight DM. At this point, the internal laser fiber was connected to a laser, which was powered on to check that the Zygo light spot and the internal laser light spot overlapped. This verified that

the optical paths overlapped enough to ensure reasonable alignment of the internal laser optical path. After the DM was installed, the flight DM driver electronics were installed and connected to the DM.

The DM was then powered on to provide zero Volts to each actuator. This served as our flat map, since the provided flat maps from the mirror manufacturer BMC were calibrated with their driver and were no longer flat using the MIT driver. The MIT driver is a miniaturized, modular PCB-based DM driver described in Haughwout 2018.[28] At this point, the beam splitter and image plane camera lens were installed, but not aligned. Then, the relay deck was installed. A corner-cube retroreflector was placed at the Shack Hartmann wavefront sensor location and the relay deck tip/tilt/rotation was adjusted with bushings until the total wavefront error throughout the system met the mission requirement of < 0.25 lambda RMS wavefront error. The final alignment measurement from the Zygo interferometer is shown in Figure 7.

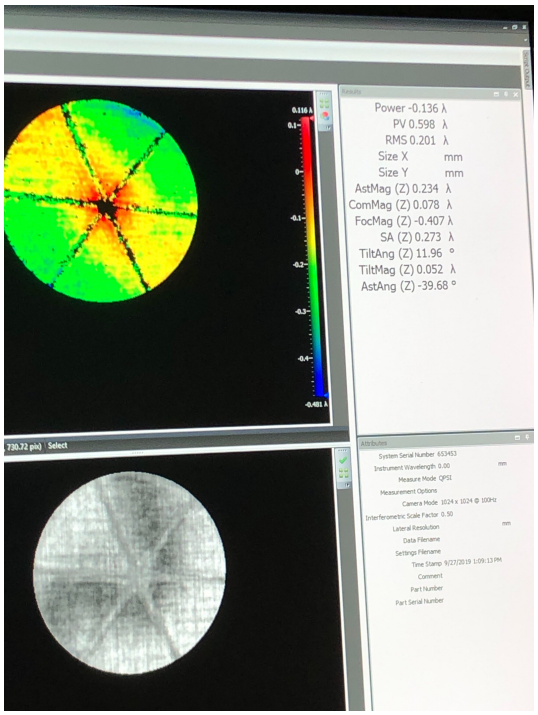

Figure 7: Final Zygo measurement of the aligned flight payload. Measurement was taken at the location of the Shack Hartmann wavefront sensor before the lenslet array was installed.

After the payload was aligned, the Shack Hartmann and Image Plane wavefront sensor cameras were installed. The image plane camera was installed by inserting its mount into the image plane lens mount and adjusting the height of the camera mount to minimize the PSF size and achieve the best focus. The set screws on the beam splitter mount were adjusted to steer the image plane PSF into the center of the image plane camera. The Shack Hartmann wavefront sensor camera was installed onto the lenslet array mount and the spot field was checked by plugging in a laser to the internal laser fiber.

Once all the optical components were installed and aligned, all screws were torqued (if they hadn't been torqued during the alignment process) and staked using 3M Epoxy Adhesive EC2216. Thermal gap filler was installed between all the optics component mounts and the optics bench, and the flight space-grade DM ribbon cables were installed into the flight DM. A picture of the full aligned payload is shown in Figure 8.

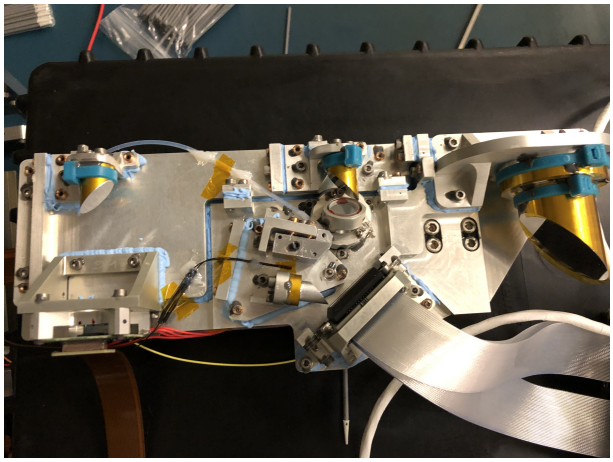

Figure 8: Fully assembled and aligned DeMi flight payload with DM ribbon cables and thermal gap filler installed.

Flight Payload Integration

After the optical bench was was fully aligned, the flight payload electronics, optics bench, and camera boards were installed into the flight bus. The entire DeMi team was instrumental in assembling the flight unit and integrating with the spacecraft bus. This process was done in several stages which are summarized here.

First, the flight electronics (including USB cables mated to the camera boards) were mated to the optics bench and command of the cameras/DM was tested.

Then, the laser diode/camera board mount was installed with the laser and attenuator installed. Then, the optical fiber between the laser and the

attenuator and between the attenuator and the connector was routed and staked into the bus with Arathane 5753 epoxy. The optical fiber that was installed into the field mirror of the payload was spliced to a connector and routed and staked into place on the payload.

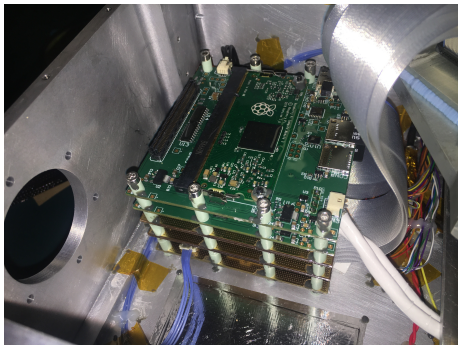

Figure 9: Electronics installed into the DeMi spacecraft bus and mated to spacecraft avionics. The optics bench is resting atop the spare optics bench feet to protect the fiber routing during installation.

Figure 10: DeMi payload fully installed into spacecraft bus.

Next, the electronics were installed, torqued, and staked into the spacecraft bus and mated to the spacecraft avionics. Figure 9 shows the electronics installed into the spacecraft bus with the optics bench resting on the spare bench feet to protect the fiber routing on the bottom of the bus. Then, the optics bench was gently lifted up so the spare feet could be removed and the optics bench was lowered into position to fit around the fiber and cable routing between the optics bench feet. Once the optics bench was in position, the feet were screwed in, torqued, and staked into place. Then, the camera boards were installed into the camera board mount and the 3d-printed baffle was installed into the spacecraft bus. Figure 10 shows the DeMi payload fully installed into the spacecraft bus before the spacecraft lid was installed. After integration, the payload was used to take measurements to validate the optical model and calibrate the wavefront sensors.

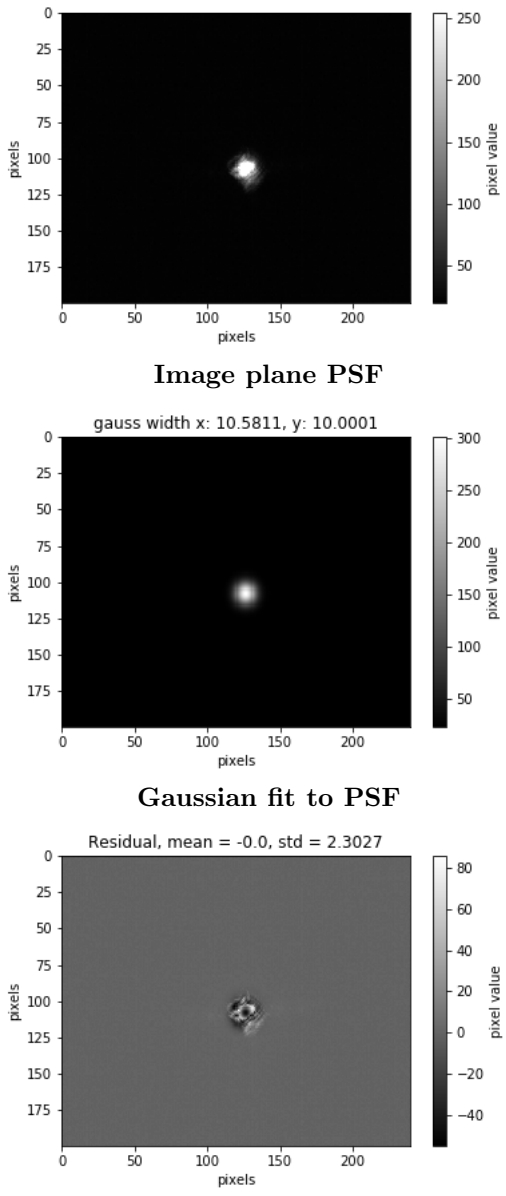

Image plane PSF

Gaussian fit to PSF

Residual (PSF - Gaussian fit)

Figure 11: Gaussian fit to measure size of image plane PSF. Measured size of spot on image plane sensor was 10.5 pixels by 10.0 pixels, after accounting for pixel binning by 2.

Optical Model Validation

The PSF on the Image Plane wavefront sensor was captured with the Image Plane camera after DeMi

was integrated with the satellite bus. In the flight measurements, pixels are binned by 2 relative to the POPPY model which assumed no binning. Figure 11 shows a zoomed-in view of the image plane PSF measurement, as well as a Gaussian fit to the PSF to measure the size of the spot on the image plane wavefront sensor. The measured spot size was 10.5 pixels by 10.0 pixels.

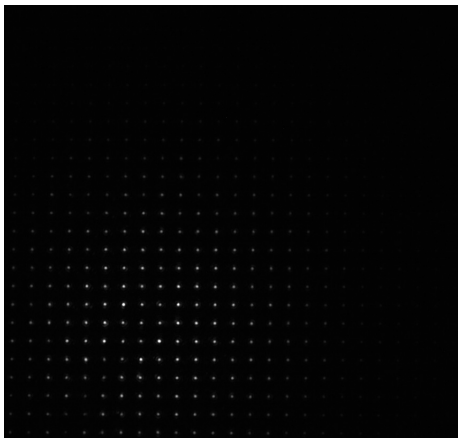

Figure 12: Measurement of spotfield on DeMi Shack Hartmann wavefront sensor after integration with satellite. Pixels are binned by 2 in this measurement.

The actual image plane PSF can be compared to the POPPY simulation shown Figure 3. The POPPY simulation assumes perfect alignment of all the elements, so the PSF is centered exactly on the sensor. In reality, not all of the optical elements were aligned to be exactly level, so the PSF is not centered on the detector exactly.

The POPPY model predicts that the image plane PSF will be an oval shape. The region illuminated by the primary spot was measured with a Gaussian fit to be 3.7 pixels by 5.3 pixels. The DeMi payload PSF was a more complicated shape, and the spot size was measured to be 10.5 pixels by 10.0 pixels across. The differences between the POPPY model and the physical payload are likely due alignment differences in the real payload. For instance, the vertical placement of the image plane sensor was performed by hand, using the spot size of the PSF to achieve the best focus. This explains why the spot size differs slightly between the POPPY model and the physical payload. The difference in shape is likely due to the small residual errors in the optical path after alignment. These results indicate that the POPPY diffraction model can be used to estimate the image plane signal, but should not be used to predict the exact measurements on the physical payload image plane sensor due to the alignment of the physical payload deviating from the idealized simulation.

The spot field from the internal calibration laser on the Shack Hartmann wavefront sensor was captured after the DeMi payload was integrated with the spacecraft bus and is shown in Figure 12. The DeMi payload sensor measurements are binned by two, so the pixel scale is different from the POPPY model outputs.

There are fewer lenslet spots illuminated with the internal calibration laser than there were in the POPPY model. This is because the POPPY model assumes an evenly illuminated plane was incident upon the primary mirror aperture to simulate the satellite observing a point source like a star. In reality, the internal calibration laser outputs a gaussian beam profile which underfills the DM slightly, which leads to this spot pattern with the illumination intensity of spots dropping off towards the edges of the beam.

The size of each lenslet spot was measured by fitting Gaussian functions to the spot measurements and using the width of the Gaussian fit to describe the size. An example spot measurement is shown in Figure 13. The average measured spot size was 3.8 pixels with a standard deviation of 0.7 pixels in x and 3.8 pixels with a standard deviation of 0.6 pixels in y. The POPPY simulation lenslet spots were measured to be 2.9 pixels by 2.9 pixels. The small difference is probably due to the alignment of the DeMi payload differing slightly from the idealized model.

The Shack Hartmann wavefront sensor was used to measure single actuator pokes of the DM. In these measurements, a single actuator is commanded to move and the centroids of the lenslet spots are recorded before and after the actuator is poked. This displacement is used to reconstruct the incident wavefront to measure the deflection of the actuator.

The x and y spot displacements are analyzed with the same zonal wavefront reconstruction function that was used to analyze simulated Shack Hartmann data. The actuator poke is then measured by fitting a Gaussian function to the reconstructed wavefront data using the Gaussfitter package in Python[3]. The actuator deflection measured is the height of the Gaussian fit to the reconstructed wavefront data. An example reconstructed wavefront measurement with corresponding Gaussian fit is shown in Figure 14. This measurement is similar to the POPPY simulation from Figure 5.

[3]https://github.com/keflavich/gaussfitter

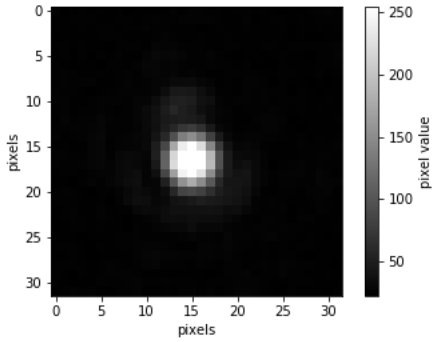

Single lenslet spot PSF

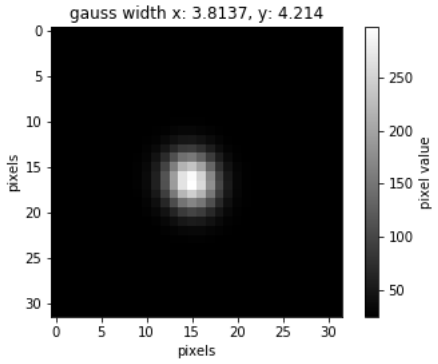

Gaussian fit to PSF

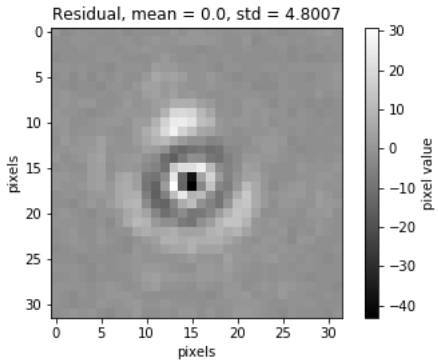

Residual (PSF - Gaussian fit)

Figure 13: Gaussian fit to measure size of single lenslet spot PSF on Shack Hartmann wavefront sensor. Measured size of spot shown was 3.8 pixels by 4.2 pixels, after accounting for the pixel binning by 2 in the measurement.

The reconstructed wavefronts from both the POPPY simulated Shack Hartmann measurements and the physical payload Shack Hartmann measurements look very similar and are well described by the Gaussian fits. The Gaussian fit to the simulation from Figure 5 had a height of 0.22 μm and a width 1.2 lenslets in x and 1.6 lenslets in y. The Gaussian fit to the flight payload measurement had a height of 0.14 μm and a width of 2.5 lenslets in x and 2.1 lenslets in y.

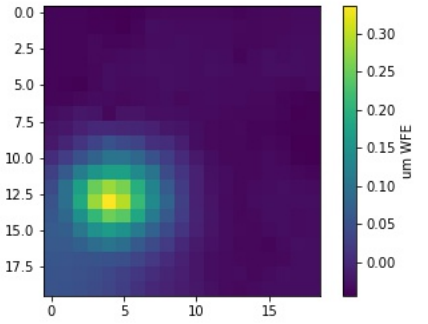

Wavefront reconstruction

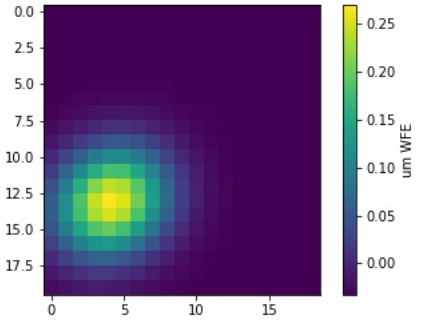

Gaussian fit to wavefront reconstruction

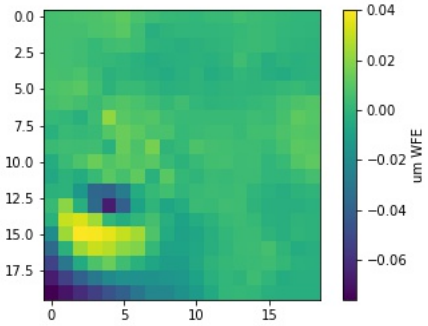

Residual (Gauss fit - reconstruction measurement)

Figure 14: Example poke measurement data analysis for actuator number 100 poked to 60 V.

The difference in height measured is due to the fact that the DM is not calibrated to deflect to a specific height, but commanded to a certain voltage, while the POPPY model inputs a deflection height. The simulation shown is comparable but not exactly the same as the deflection from the physical DM in

the payload, since the Shack Hartmann wavefront sensor calibration is still ongoing. The small difference in width between the simulation and the DeMi payload data could be due to the actual influence funtion of the DeMi DM deviating slightly from the model used in the POPPY model, or due to the difference in alignment between the actual DeMi payload and the idealized POPPY model.

Conclusions

A POPPY diffraction model has been developed using the POPPY package in Python to predict measurements from the DeMi CubeSat payload. The flight payload alignment and integration was summarized, and measurements from the flight payload were compared to the diffraction model results.

The POPPY diffraction model has been validated for both the image plane and the Shack Hartmann sensor. The model can be used to estimate the signal on either sensor. Since the POPPY model does not account for the actual alignment of the physical payload, the simulation results differ slightly from the actual data from the payload. The model will be useful for predicting the effects of the incline of the DM in the payload on the wavefront sensor measurements.

The DeMi CubeSat was successfully launched to the International Space Station in February 2020. Deployment from the station is expected in Spring/-Summer 2020. After deployment, the satellite will undergo a brief commissioning period to establish communications and operations protocols. Then, payload operations will begin. The optical model and image processing code developed in this work will be used to calibrate and analyze flight data from the DeMi payload and monitor the behavior of the MEMS DM on-orbit.

Acknowledgements

The DeMi mission is funded by DARPA and managed by Aurora Flight Sciences, a Boeing Company.

The author is sponsored by a NASA Space Technology and Research Fellowship. The optical simulations were performed on the Engaging cluster at the MGHPCC facility (www.mghpcc.org).

References

[1] W. A. Traub, B. R. Oppenheimer, and S. Seager (Ed.), "Direct Imaging of Exoplanets," in *Exoplanets*, 2010, pp. 111–156.

[2] G. Chauvin, A.-M. Lagrange, H. Beust, *et al.*, "Orbital characterization of the Beta Pictoris b giant planet," *Astronomy & Astrophysics*, vol. 542, A41, 2012, ISSN: 0004-6361. DOI: 10.1051/0004-6361/201118346.

[3] B. R. Oppenheimer, C. Baranec, C. Beichman, *et al.*, "Reconnaissance of the hr 8799 exosolar system. I. near-infrared spectroscopy," *Astrophysical Journal*, vol. 768, no. 24, 2013, ISSN: 15384357. DOI: 10.1088/0004-637X/768/1/24.

[4] P. Kalas, J. R. Graham, M. P. Fitzgerald, *et al.*, "Stis coronagraphic imaging of fomalhaut: Main belt structure and the orbit of fomalhaut b," *Astrophysical Journal*, vol. 775, no. 56, 2013, ISSN: 15384357. DOI: 10.1088/0004-637X/775/1/56.

[5] S. Seager and D. Deming, "Exoplanet Atmospheres," *Annual Review of Astronomy and Astrophysics*, vol. 48, pp. 631–672, 2010, ISSN: 0066-4146. DOI: 10.1146/annurev-astro-081309-130837.

[6] M. C. Wyatt, "Evolution of Debris Disks," *Annual Review of Astronomy and Astrophysics*, vol. 46, no. 1, pp. 339–383, 2008, ISSN: 0066-4146. DOI: 10.1146/annurev.astro.45.051806.110525.

[7] B. Crill, N. Siegler, S. Domagal-goldman, *et al.*, "Key Technology Challenges for the Study of Exoplanets and the Search for Habitable Worlds," Tech. Rep., 2018. [Online]. Available: https://arxiv.org/pdf/1803.04457.pdf.

[8] B. Nemati, M. T. Stahl, H. P. Stahl, *et al.*, "Effects of space telescope primary mirror segment errors on coronagraph instrument performance," in *Proceedings of SPIE 10398 UV/Optical/IR SPace Telescopes and Instruments: Innovative Technologies and Concepts VIII*, 2017. DOI: 10.1117/12.2273072.

[9] F. Malbet, W. Yu J., and M. Shao, "High-Dynamic-Range Imaging Using a Deformable Mirror for Space Coronography," *Publications of the Astronomical Society of the Pacific*, vol. 107, pp. 386–398, 1995.

[10] L. Pueyo and N. J. Kasdin, "Polychromatic Compensation of Propagated Aberrations for High-Contrast Imaging," *The Astrophysical Journal*, vol. 666, no. 1, pp. 609–625, 2007, ISSN: 0004-637X. DOI: 10.1086/518884.

[11] H. W. Babcock, "The Possibility of Compensating Astronomical Seeing," *Publications of the Astronomical Society of the Pacific*, vol. 65, no. 386, pp. 229–236, 1953.

[12] N. Jovanovic, O. Absil, P. Baudoz, *et al.*, "Review of high-contrast imaging systems for current and future ground-based and space-based telescopes II. Common path wavefront sensing/control and Coherent Differential Imaging," in *Proceedings of SPIE Astronomical Telescopes and Instrumentation*, 2018.

[13] K. M. Morzinski, J. W. Evans, S. Severson, *et al.*, "Characterizing the potential of MEMS deformable mirrors for astronomical adaptive optics," in *Proceedings of SPIE 6272 Advances in Adaptive Optics II*, 2006. DOI: 10.1117/12.672470.

[14] M. A. Helmbrecht, M. He, C. J. Kempf, *et al.*, "MEMS DM development at Iris AO, Inc.," in *Proceedings of SPIE 7931 MEMS Adaptive Optics V*, 2011. DOI: 10.1117/12.876186.

[15] R. Morgan, E. Douglas, G. Allan, *et al.*, "MEMS Deformable Mirrors for Space-Based High COntrast Imaging," *Micromachines*, vol. 10, no. 306, 2019. DOI: doi:10.3390/mi10060366.

[16] K. L. Cahoy, A. D. Marinan, B. Novak, *et al.*, "Wavefront control in space with MEMS deformable mirrors for exoplanet direct imaging," *Journal of Micro/Nanolithography, MEMS, and MOEMS*, vol. 13, no. 1, 2014, ISSN: 1932-5150. DOI: 10.1117/1.jmm.13.1.011105.

[17] A. Marinan and K. Cahoy, "CubeSat Deformable Mirror Demonstration," in *International Symposium on Optomechatronic Technologies*, 2014.

[18] A. Marinan, K. Cahoy, J. Merck, *et al.*, "Improving Nanosatellite Imaging with Adaptive Optics," in *Proceedings of AIAA/USU Conference on Small Satellites*, 2016.

[19] E. S. Douglas, G. Allan, D. Barnes, *et al.*, "Design of the deformable mirror demonstration CubeSat (DeMi)," in *Proceedings of SPIE 10400 Techniques and Instrumentation for Detection of Exoplanets*, 2017. DOI: 10.1117/12.2274430.

[20] E. S. Douglas, G. Allan, D. Barnes, *et al.*, "Design of the deformable mirror demonstration CubeSat (DeMi)," in *Proceedings of SPIE 10400 Techniques and Instrumentation for Detection of Exoplanets*, 2017. DOI: 10.1117/12.2274430.

[21] G. W. Allan, *Simulation and Testing of Wavefront Reconstruction Algorithms for the Deformable Mirror (DeMi) Cubesat. Master's Thesis, Massachusetts Institute of Techonology*, 2018.

[22] G. Allan, E. S. Douglas, D. Barnes, *et al.*, "The deformable mirror demonstration mission (DeMi) CubeSat: optomechanical design validation and laboratory calibration," vol. 1069857, no. August 2018, p. 180, 2018. DOI: 10.1117/12.2314192.

[23] M. D. Perrin, R. Soummer, E. M. Elliott, *et al.*, "Simulating point spread functions for the James Webb Space Telescope with WebbPSF," in *Space Telescopes and Instrumentation 2012: Optical, Infrared, and Millimeter Wave*, M. C. Clampin, G. G. Fazio, H. A. MacEwen, *et al.*, Eds., International Society for Optics and Photonics, vol. 8442, SPIE, 2012, pp. 1193–1203. DOI: 10.1117/12.925230. [Online]. Available: https://doi.org/10.1117/12.925230.

[24] E. Hecht, *Optics 5th Edition*. Pearson Education Limited, 2017.

[25] W. Southwell, "Wave-front estimation from wave-front slope measurements," *J. Opt. Soc. Am.*, vol. 70, no. 8, pp. 998–1006, Aug. 1980. DOI: 10.1364/JOSA.70.000998. [Online]. Available: http://www.osapublishing.org/abstract.cfm?URI=josa-70-8-998.

[26] G.-m. Dai, *Wavefront Optics for Vision Correction*. SPIE, 2008. DOI: https://doi.org/10.1117/3.769212.

[27] J. Gubner, *Deformable Mirror Demonstration Mission. Bachelor's Thesis, Wellesley College Honors Thesis Collection. 606.* 2018. [Online]. Available: https://repository.wellesley.edu/thesiscollection/606.

[28] C. Haughout, *Electronics Development for the Deformable Mirror Demonstration Mission (DeMi). Master's Thesis, Massachusetts Institute of Technology*, 2018.